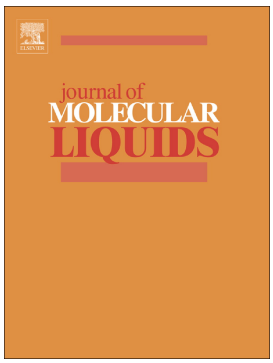

High-performance symmetric supercapacitor; nanoflower-like NiCo2O4//NiCo2O4 thin films synthesized by simple and highly stable chemical method

S.K. Shinde, H.M. Yadav, Sivalingam Ramesh, C. Bathula, Nagesh Maile, G.S. Ghodake, Haridas Dhaygude, D.-Y. Kim

PII: S0167-7322(19)34085-1

DOI: https://doi.org/10.1016/j.molliq.2019.112119

Reference: MOLLIQ 112119

To appear in: *Journal of Molecular Liquids*

Received date: 22 July 2019

Revised date: 6 November 2019

Accepted date: 11 November 2019

Please cite this article as: S.K. Shinde, H.M. Yadav, S. Ramesh, et al., High-performance symmetric supercapacitor; nanoflower-like NiCo2O4//NiCo2O4 thin films synthesized by simple and highly stable chemical method, *Journal of Molecular Liquids*(2018), https://doi.org/10.1016/j.molliq.2019.112119

High-Performance Symmetric Supercapacitor; Nanoflower-Like $NiCo_2O_4$//$NiCo_2O_4$ Thin Films Synthesized by simple and highly stable chemical method

S. K. Shinde[a], H. M. Yadav[b], Sivalingam Ramesh[c], C. Bathula[d], Nagesh Maile[e], G. S. Ghodake[a], Haridas Dhaygude[f], D. -Y. Kim[a]*

[a]*Department of Biological and Environmental Science, College of Life Science and Biotechnology, Dongguk University, 32 Dongguk-ro, Biomedical Campus, Ilsandong-gu, Siksa-dong, 10326, Goyang-si, Gyeonggi-do, South Korea*

[b]*Department of Energy and Materials Engineering Dongguk University Seoul, 04620, South Korea.*

[c]*Department of Mechanical, Robotics and Energy Engineering, Dongguk University-Seoul, Pildong, Jung-gu, 04620, Seoul, Republic of Korea.*

[d]*Division of Electronics and Electrical Engineering, Dongguk University –Seoul, Pil-dong, Jung-gu, 04620, Seoul, South Korea.*

[e]*Department of Environmental Engineering, Kyungpook National University, 80 Daehak-ro, Buk-gu, Daegu 41566, South Korea*

[f]*Department of Physics, Doodhsakhar Mahavidyalaya, Bidri*

***Corresponding Author: Prof. D. –Y. Kim**

Tel: +82-31-961-5122

Fax: +82-31-961-5122

Mobile: +82-10-6658-5213

E-mail: sbpkim@gmail.com; surendrashinde.phy@gmail.com

Abstract

In this study, flowers-like interconnected nanoflakes $NiCo_2O_4$ thin films were synthesized by the SILAR method for the fabrication of supercapacitor application. X-ray diffraction analysis revealed that the synthesized $NiCo_2O_4$ thin films exhibit polycrystalline nature, and FE-SEM images confirmed their highly porous-like surface area. The analysis of structural, elemental, and compositional properties of the $NiCo_2O_4$ thin films were confirmed, that the thin films were used as electrode material for supercapacitor applications used as electrode material for supercapacitor testing. As expected, the prepared $NiCo_2O_4$ thin films showed high stability and served as efficient materials for use in supercapacitors application. The $NiCo_2O_4$ thin films exhibited excellent cycling charge-discharge with a specific capacitance (C_S) of 1936 F g^{-1} at a scan rate of 5 mV s^{-1} in a 3 M KOH electrolyte. Cycling stability results revealed that $NiCo_2O_4$ thin films exhibit highly stable performance with a 94.5% retention. Symmetric supercapacitor performance presenting an energy density of 294.54 kWh kg^{-1} and power density 7.8 W kg^{-1}, it indicates the $NiCo_2O_4$ based electrode is applicable for the practical applications in device fabrication of asymmetric and symmetric supercapacitor. The high performance of the $NiCo_2O_4$ thin films is possibly related to the presence of a highly porous surface morphology and stepwise effects of the SILAR cycle.

Keywords: Chemical synthesis, $NiCo_2O_4$ thin film, Nanoflower, Different nanostructures, Electrochemical study.

1. Introduction

Supercapacitors have demonstrated promise as electronic devices for energy storage applications and challenges over last several years due to their compact size, higher electrical conductive nature along with excellent charging-discharging rate and long-term stability compared to capacitors and batteries [1-4]. Currently, various binary metal oxide and sulfide electrodes have been utilized in applications of energy storage devices like supercapacitors [5] due to their extraordinary properties such as high energy density as well as power density, lightweight nature, small size, and long-term cycling stability. To enhance the electrochemical performance compared to binary metal oxides or sulfides, ternary composites of $NiCo_2O_4$ thin films are considered as superior for the supercapacitor application.

Recently, various ternary metal oxides/sulfides have been prepared by different methods for supercapacitor applications, including $MnCo_2O_4$ [6], $CoFe_2O_4$ [7], $NiCoO_4$ [8], FeCoO/ polyaniline [9], $(Co_{0.5}Fe_{0.5})_3O_4$ [10], and $NiCo_2S_4$ [11]. Of these metal oxides/sulfides. The selected $NiCo_2O_4$ thin films have been utilized for various applications due to their higher electrical conductivity as well as higher performance and long-term stability. Synthesized $NiCo_2O_4$ thin films have been utilized in various applications, including solar cells [12], Li-ion batteries [13], supercapacitor capacitor [14, 15], water spitting [16], hydrogen evolution [17], gas sensing [18], oxygen evolution [19], non-enzyme glucose detection [20], and electrocatalyst [21], using different methods reported previously. Previously, various $NiCo_2O_4$ nanostructures have been prepared by different methods for supercapacitor applications. For example, nanorods (980 F g^{-1} at a current density of 2 A g^{-1}) [22], nanowires (1242 F g^{-1} at a current density of 10 mA cm^{-2}) [23], nanoflakes (1811 F g^{-1} at a current density of 0.5 mA cm^{-2}) [24], nanosheets

(199.74 F cm^{-3} at a current density of 0.2 mA cm^{-2}) [25], nanosheets (790 F cm^{-3} at 1.43 g cm^{-3}) [26], nanotube/wire (693.6 F g^{-1} at a current density of 6.66 A g^{-1}) [27], nanotubes (828 F g^{-1} at 1 A g^{-1}) [28], blooming flowers (1545 F g^{-1} at a current density of 5 A g^{-1}) [29], sea urchin [30], nanoparticles (1335 F g^{-1} at a current density of 30 A g^{-1}) [31], and urchin (F g^{-1} at a current density of 15 A g^{-1}) [32]. An interconnected nanoflakes-like flower nanostructure was prepared for supercapacitor applications. The high surface area and easy ion transformation provided by these nanoflowers-like nanostructures during electrochemical analysis. In addition, inexpensive SILAR is not only a facile method but also the most useful method for the deposition of nanomaterials on a flexible steel substrate. Furthermore, SILAR is beneficial to grow various nanostructures by the adjustment of simple preparation parameters [33, 34].

In this study, three different porous nanostructures of $NiCo_2O_4$ thin films were prepared by controlling the simple deposition parameters of the SILAR method. The effect of deposition cycles was systemically investigated by structural, morphological, and electrical studies. $NiCo_2O_4$ thin films with a nanoflowers-like surface morphology were synthesized by a simple, reproducible, and eco-friendly approach. Results shown that the deposition cycles are effected on the structural, morphological, and supercapacitive properties of the $NiCo_2O_4$ thin films. The interconnected flower-like $NiCo_2O_4$ nanostructures provided the highest C_S of 1936 F g^{-1} at a scan rate of 5 mV s^{-1} with superior cycling stability.

2. Experimental details

2.1 Materials:

Nickel(II) perchlorate hexahydrate ($Ni(ClO_4)_2 \cdot 6H_2O$), cobalt (II) perchlorate hexahydrate ($Co(ClO_4)_2 \cdot 6H_2O$) were purchased from Daejung Chemicals (South Korea), and ammonia (25%)

was purchased from Wako Pure Chemical Industries (Osaka, Japan). All chemicals were used as received.

2.2 Preparation of $NiCo_2O_4$ thin films:

To deposit the $NiCo_2O_4$ thin films, 0.1 M nickel perchlorate hexahydrate as the cationic precursor and 0.1 M cobalt perchlorate hexahydrate as the anionic precursor were first dissolved in ammonia at pH 11. Second, the well-cleaned flexible stainless-steel substrate was dipped into $Ni(ClO_4)_2$ for 20 s to deposit Ni^{2+} on it. Third, the flexible stainless-steel substrate was washed in double-distilled water for 5 s to eliminate roughly bound Ni^{2+} species, followed by dipping into the $Co(ClO_4)_2$ solution to deposit Co^{2+} species at room temperature for 20 s, affording a widespread coating of the $NiCo_2O_4$ thin films. Next, the flexible stainless-steel substrate was cleaned in double-distilled water for 5 s to separate loosely bound Ni^{2+} and Co^{2+} species [11, 34]. Hence, the SILAR cycle of $NiCo_2O_4$ thin films is established, and various cycles were repeated to obtain the desired $NiCo_2O_4$ film thickness obtained as a result of 15, 25, and 35 deposition cycles and annealing theses samples to 300 $^{\circ}$C for 1 hr., which are hereafter referred to as NCO:A, NCO:B, and NCO:C, respectively. The active mass loading for NCO:A, NCO:B, and NCO:C samples were found to 0.31, 0.39, and 0.34 mg/cm^2, respectively.

2.3 Characterizations

The structures of the $NiCo_2O_4$ thin films were investigated by using a X-ray diffractometer (Bruker D8 Advance) with Cu-K_α radiation (λ=1.54 Å). The morphologies and microstructures of the films were observed by field-emission scanning electron microscopy (FE-SEM, Mira-3, Tescan Pvt. Brno-Czech Republic) and high-resolution transmission electron microscopy (HR-TEM; FEI, Titan G2 Chemi STEM Cs Probe). X-ray photoelectron spectroscopy (XPS, ULVAC-PHI Quantera SXM) was used to confirm chemical composition of

the films. The elemental analysis of samples was examined by energy-dispersive X-ray spectroscopy (EDS, Oxford Instruments), inbuilt in the FE-SEM system. Electrochemical analyses were carried out with a CHI 660D electrochemical workstation [11].

2.4 Electrode preparation and electrochemical measurements

The electrochemical characteristics of the $NiCo_2O_4$ thin films were assessed by measuring cyclic voltammetry (CV), galvanostatic charge/discharge (GCD), and electrochemical impedance (EIS). Electrochemical performance was analyzed in 3 M KOH solution with a three-electrode cell configuration including flexible $NiCo_2O_4$ films, platinum, and Ag/AgCl as the working, counter, and reference electrodes, respectively [11]. CV measurements were carried out at different scan rates in a potential window of –0.1 to 0.5 V, and charge–discharge characteristics at different current densities within the same potential window were investigated. EIS analyzed in between 1 Hz and 100 kHz with an alternate current (AC) amplitude of 10 mV and a bias potential of 0.4 V.

2.5 Fabrication of $NiCo_2O_4$//$NiCo_2O_4$ flexible symmetric devices

The flexible symmetric $NiCo_2O_4$//$NiCo_2O_4$ electrodes were bring together as positive and negative probs. The two electrodes were separated with a filter paper, and gel of PVA/KOH was used as the electrolyte. The preparation of PVA/KOH gel and device fabrication is described in our recent reports [35]. Both of the prepared electrodes and separator paper was dipped into the gel electrolyte for 5 s and then dried in air at 25 $^{\circ}$C for 12 h. Finally, these electrodes were pasted with PVA/KOH gel electrolyte before the device assembling and kept for drying 6 h at 35 °C in an electric oven to remove adsorbed water from the surface. In the next step symmetric device was assembled by pressing the pasted region of electrodes and kept a pressure of 1 ton for 1 h, to enhance the interface of electrolyte to the electrode surface [1, 35].

3. Results and Discussion

3.1 X-ray diffraction (XRD) study

XRD patterns were recorded to determine the crystal structure and phase confirmation of the synthesized ternary $NiCo_2O_4$ thin films at various SILAR cycles. Figure S1 (a-c) shows the typical XRD patterns of the $NiCo_2O_4$ thin films deposited on a flexible stainless-steel substrate by using different SILAR cycles. Figure 1a shows the optimized XRD pattern of the pure $NiCo_2O_4$ thin films, without impurities in these thin films was observed [36, 37]. Peaks observed at 17.26°, 31.96°, 34.45°, 44.03° and 74.85°, corresponded to the (111), (220), (311), (400) and (620) planes of $NiCo_2O_4$ (JCPDS card number 073-1702), respectively, and peaks observed at 24.53°, 44.03° and 74.85° are attributed to the stainless steel substrate material., similar types of crystal structures are reported in previous study [36-38]. As shown in Figure S1 (a-c), deposition cycles increase the peak intensity of diffraction peaks increases up to 25 cycles, future that the peak intensity decreases. Because of the film peeled off from the substrate of the $NiCo_2O_4$ thin films at 35 deposition cycle. Crystallite sizes were calculated using the Scherrer equation for the peak at 34.45° corresponding to the $NiCo_2O_4$ thin films, indicative of the different crystallite values of these $NiCo_2O_4$ thin films. The calculated crystallite sizes for NCO:A, NCO:B, and NCO:C were 70, 66, and 80 nm, respectively. The crystallite size of the $NiCo_2O_4$ thin films is in the range of few nanometers (nm). These results agree with the SEM and TEM studies described in section 3.3 and 3.4, respectively. The low crystallite size values revealed that these samples are beneficial for the current collector measurement due to the thin surface of the $NiCo_2O_4$ samples. In addition, lattice parameters were calculated by using the following standard relation [39].

$$a = d\,(h^2 + k^2 + l^2)^{1/2} \quad (1)$$

The lattice parameter values for NCO:A, NCO:B, and NCO:C thin films were 8.13, 8.59, and 8.72 Å, respectively. The standard and calculated values are slightly greater than the calculated values [40]. NCO:A exhibited a slightly lower difference between the standard and calculated values, indicating that NCO:A is well formation with stoichiometric $NiCo_2O_4$ phase.

3.2 X-ray photoelectron spectroscopy (XPS) study

XPS analysis was employed to obtain information regarding the elemental, chemical, and oxidation valence of the optimized $NiCo_2O_4$ samples. Figure 1b demonstrate the XPS survey spectrum of the $NiCo_2O_4$ thin films prepared by the SILAR method at 25 deposition cycles. Ni, Co, and O were observed in the prepared $NiCo_2O_4$ sample, confirming the successful formation of the $NiCo_2O_4$ thin films (Figure 1b). The narrow scan XPS was further utilized to acquire the detailed information of Ni, Co, O element in the thin film as show in Figure 1 (c-e). The Ni 2p spin-orbit doublet peaks observed at 855.49 eV and 873.11 eV corresponded to Ni^{2+} with two shake-up satellite peaks is shown in Figure 1c [41]. Similar two peaks were observed at 780.90 eV and 796.46 eV corresponded to Co $2p_{3/2}$ and Co $2p_{1/2}$, respectively (Figure 1d) [42]. Figure 1e shows the O1s narrow scan XPS spectrum. A binding energy peak observed at 530.80 eV corresponded to the O1s metal-oxide energy state, indicative of the presence of oxygen in the as-prepared samples [43, 44].

3.3 Field-emission scanning electron microscopy study

After the confirmation of pure phase of the $NiCo_2O_4$ thin films using XRD and XPS results, FE-SEM were used for examination of the surface morphology of the synthesized $NiCo_2O_4$ thin films with different deposition cycles (Figure 2). The FE-SEM images of the $NiCo_2O_4$ thin films prepared at various SILAR cycles of 15, 25, and 35 with different magnifications are shown in Figure 2 (a–f). The flexible substrate was completely and uniformly

covered with different nanostructures at different deposition cycles (Figure 2 (a–f)). At the lower deposition cycle of 15, $NiCo_2O_4$ was agglomerated with several irregular nanosheets, and a nanoparticle-like nanostructure was deposited on the flexible substrate, possibly related to the incompletely deposition of the $NiCo_2O_4$ on the flexible substrate. To overcome this issue, the number of deposition cycles were increased from 15 to 25 for the complete growth of the $NiCo_2O_4$ thin films [45]. Figure 2 (c, d) shows the typical surface morphology of the $NiCo_2O_4$ thin films, the hierarchical nanostructure comprised different-sized nanoflakes with comparatively highly porous surfaces. The high-magnification image revealed the presence of an interconnected nanoflowers-like nanostructure covered on the flexible substrate [46]. FE-SEM analysis confirmed that interconnected vertical grow of nanoflakes-like flower $NiCo_2O_4$ thin films are grown on the sample with a thickness of 9–15 nm. This type of surface morphology provided a highly porous and reactive surface area for the sample, indicating that this sample is more suitable than the other two samples. To increase in the number of deposition cycles from 25 to 35, nanostructure developed large size sheets of the $NiCo_2O_4$ thin films were deposited on the substrate with a thickness of 30–50 nm and the length of 500–600 nm (Figure 2 (e, f)). Uniform, highly porous nanoflower nanosurfaces were observed, with a lower values solution and charge-transfer resistance, revealing that the $NiCo_2O_4$ electrode is more suitable for electrochemical applications (Figure 2 (a-f)) [45-47]. Figure 2 (g-i) displays the EDS micro images of the $NiCo_2O_4$ thin films prepared at different SILAR cycles, respectively. All samples revealed the presence of Ni, Co, and O, confirming the formation of the $NiCo_2O_4$ thin films [46].

3.4 TEM and HR-TEM study

TEM images of the $NiCo_2O_4$ thin films deposited at different cycles were recorded to obtain in-depth details of the surface morphology of $NiCo_2O_4$ samples and are shown in Figure 3

(a-c). All the samples exhibited a porous-like surface morphology with different-sized nanosheets, providing the more rapid transfer of ions, superior electrochemical reaction, and more active species [48]. From TEM images, with the increase in the number of deposition cycles, more porous, uniform nanostructures were observed on the surface (Figure 3 (a–c)). Among these samples, the middle $NiCo_2O_4$ samples exhibited better porosity and a lower thickness of 5–6 nm, suggesting that $NiCo_2O_4$ samples provide more surface area during the contact between the liquid KOH electrolyte and $NiCo_2O_4$ electrode, easily favoring the transport of mass from the interface between the electrolyte and electrode for supercapacitors; this favorable mass transport can improve the device performance [49]. Figure 3 (d-g) shows the HR-TEM images of optimized NCO:B sample with different magnification, d-spacing, and the SAED pattern, respectively. The NCO:B sample clearly shows the chain of flowers like nanostructures developed on surface of the steel substrate (shown in figure 3d), and these flowers showing more porous with 3-5 nm thickness and SAED pattern images of $NiCo_2O_4$ thin film as seen in Figure 3f and 3g, respectively. Figure 3 (h-k) shows the elemental mapping of NCO:B sample. The elemental mapping clearly shows the Ni, Co and O elements are uniform distribution on the surface of NCO:B sample. The TEM, HR-TEM and mapping analysis are in good agreement with the FE-SEM and EDS results [35, 50, 51].

3.5. Electrochemical supercapacitive properties

3.5.1 Supercapacitive Studies

After the structural, morphological, and compositional analyses of the $NiCo_2O_4$ films were confirmed, CV and GCD measurements were carried out to further investigate the electrochemical supercapacitive properties. CV curves of the as-prepared $NiCo_2O_4$ electrodes were recorded at varying scan rates of 5–100 mV s^{-1} within a potential of –0.1 to 0.5 V in a 3 M

KOH electrolyte. Figure S2 (a, c) shows the CV curves and calculated C_S for the NCO:A, NCO:B, and NCO:C electrodes. NCO:B electrode exhibited the highest specific capacitance [50, 51]. It also exhibited a considerably greater CV internal surface area than the other two electrodes, indicating that the interconnected nanoflowers-like nanostructure provide a more surface active area, and a higher reactive area is helpful for the exchange of ions in the electrodes [52]. Figure 4 (a–c) shows the CV curves of the $NiCo_2O_4$ electrodes at different scan rates from 5 to 100 mV s^{-1} within the potential window from −0.1 to 0.5 V. These CV curves revealed that NCO:B exhibits a considerably higher internal surface area than NCO:A and NCO:C samples, indicative of the higher specific capacitance for NCO:B. The anodic and cathodic peaks moved to the positive and negative windows, respectively, and vice versa, indicative of the pseudocapacitive behavior of the $NiCo_2O_4$ electrodes (Figure 4 (a-c) and Figure S2a) [32]. Figure 4d shows the specific capacitance as a function of various scan rates from 5 to 100 mV s^{-1} of the $NiCo_2O_4$ electrodes. The specific capacitance (C_S) of the $NiCo_2O_4$ electrodes was calculated by the following standard equation [52]:

$$C_S = \frac{1}{mv(V_c - V_a)} \int_{V_a}^{V_c} I(V)dv \tag{2}$$

where, C_S is the specific capacitance (F g^{-1}), n is the potential scan rate (mV s^{-1}), (V_c–V_a) is the potential range (−0.1 to 0.5 V), I is the current response (mA), and m is the deposited mass of the $NiCo_2O_4$ electrodes. The calculated C_S values for NCO:A, NCO:B, and NCO:C were 799 F g^{-1}, 1936 F g^{-1}, and 1376 F g^{-1}, respectively, at a scan rate of 5 mVs^{-1} (Figure 4d). From the C_S values, NCO:B exhibited better performance than the other two electrodes due to the higher reactive surface area and highly porous thin nanoflakes-like nanostructure, indicative of the maximum specific capacitance [51]. The specific capacitance values for the NCO:A electrode

were 799, 483, 256, 184, 138, and 106 F g^{-1}. The corresponding values for NCO:B and NCO:C were 1936, 1306, 916, 778, 735, 680 F g^{-1} and 1376, 821, 568, 388, 376, 364 F g^{-1}, respectively. The comparative lower C_S values for the other two electrodes were related to the lower active area, higher solution resistance, and thickness of the nanostructure. Such a nanostructures supplied a low rate in the ion-exchange mechanism.

3.5.2 Galvanostatic Charge–Discharge (GCD) Study

To obtain further detailed information and relationship between the $NiCo_2O_4$ electrodes and supercapacitor, GCD measurements were carried out within the potential window from –0.1 to 0.5 V in 3 M KOH electrolytes at different current densities. The charging–discharging times for NCO:A, NCO:B, and NCo:C were 463, 1510, and 1304 s, respectively, at a current density of 10 mA cm^{-2} (Figure S2b). The charging–discharging times revealed that NCO:B exhibits the maximum discharging time, strongly indicative of the maximum specific capacitance. Figure 5 (a-c) shows the GCD curves of NCO:A, NCO:B, and NCO:C at various current densities from 10 to 35 mA cm^{-2}. The Cs of the electrode was calculated using the following equation [52];

$$C_S = \frac{I\Delta t}{m\Delta V} \tag{3}$$

where, I (mA) is the discharge current for the applied time duration Δt (s), ΔV (V) is the potential window, and m is the weight of the electrodes. The calculated capacitance values from the charging/discharging times were 356, 204, 136, 85, 72, and 49 F g^{-1} for NCO:A; 1436, 1059, 814, 580, 472, and 385 F g^{-1} for NCO:B; and 1200, 900, 569, 306, 255 and 205 F g^{-1} for NCO:C at current densities of 10, 15, 20, 25, 30, and 35 mA cm^{-2}, respectively (Figure 5d). NCO:B exhibited higher C_S than NCO:A and NCO:C samples, respectively (Figure 5d). NCO:B exhibited the maximum C_S values of 1438 F g^{-1} at 10 mA cm^{-1} and 385 F g^{-1} at 35 mA cm^{-1},

suggestive of a loss of only 10% at higher current density. This result demonstrated that NCO:B can serve as a better supercapacitor than the other $NiCo_2O_4$ samples because the nanoflowers-like surface morphology provides more rapid pathways for electron transfer, porous surface area, and death of penetration [53]. The specific capacitance values obtained herein are superior to that reported previously for nanocoral-like $NiCo_2O_4$ (870.7 F g^{-1}) [54]. Cycling stability is a key factor in the investigation of supercapacitor properties for the device frication application. Figure 5e shows the Cs of the optimized $NiCo_2O_4$ electrode at a constant scan rate of 100 mV s^{-1} with a function of the number of cycles. The calculated C_S of the optimized $NiCo_2O_4$ electrode on the flexible steel substrate continuously increased up to the first 200 cycles, followed by the slow decrease [55, 56]. In additional, a capacitance retention of 94.5% after 1000 cycles was observed for the $NiCo_2O_4$ electrodes, confirming that the nanoflowers-like $NiCo_2O_4$ electrodes exhibit superior [5] properties compared to the other reported nanostructures as the flowers-like nanostructure supplies several interconnected nanoflakes with a more porous-like surface morphology. Stability results confirmed that the flower-like $NiCo_2O_4$ electrodes exhibit good long-term stability [57-60].

3.5.3 EIS measurements

EIS measurements were carried for the $NiCo_2O_4$ electrodes synthesized at various deposition cycles. Figure 5f shows the Nyquist plots of the $NiCo_2O_4$ electrodes prepared at different deposition cycles [32]. Solution resistance (R_s) values for the NCO:A, NCO:B, and NCO:C electrodes were 2.9, 1.94, and 3.8 Ω, respectively, with corresponding charge-transfer resistance (R_{ct}) values of 8.6, 3.2, and 4.6 Ω. Table 1 summarizes the R_s and R_{ct} values: NCO:B exhibited R_s and R_{ct} values almost one half those of the other two electrodes. From the EIS

result, NCO:B is confirmed to exhibit lower R_s and R_{ct} values, indicating that NCO:B is more beneficial for the transport of ions and electrons [52, 58-60].

3.6 Device fabrication for $NiCo_2O_4$//$NiCo_2O_4$ symmetric supercapacitor

The $NiCo_2O_4$//$NiCo_2O_4$ symmetric supercapacitor was assembled using interconnected nanosheets as positive and negative electrodes, paper as a separator, and a KOH gel as the electrolyte (Figure 6a). Figure 6b shows the CV of the $NiCo_2O_4$//$NiCo_2O_4$ cell in the potential window from 0 to 0.6 V at various scan rates from 10 to 100 mV s^{-1}. The CV curves demonstrate redox and oxidation peaks at all of the investigated scan rates, which is related to the redox reactions between the positive/negative $NiCo_2O_4$ electrode and the KOH gel electrolyte [61-64]. Similar results were observed in the GCD curves recorded at different current densities of 6-10 mA cm^{-2}. Figure 6d shows the GCD curves of the $NiCo_2O_4$//$NiCo_2O_4$ symmetric supercapacitor in the potential of 0 to 0.6 V. This figure shows that the voltage (IR) drops are very small, indicating that the $NiCo_2O_4$//$NiCo_2O_4$ symmetric supercapacitor is highly conductive; this property favors good supercapacitor performance. Figure 6 (c, e) shows the C_S at various scan rates from 10 to 100 mV s^{-1} and at different current densities from 6 to 10 mA cm^{-2}, respectively. The symmetric supercapacitor cell shows a specific capacitance approximately 116 F g^{-1} greater than the specific capacitance value previously reported for a sulfide-based symmetric/asymmetric supercapacitor cell [65-67]. One of the most significant parameters for appreciative the practical applications and fabricating supercapacitor devices with good energy storage performance and long-term cycling stability [68]. Figure 6 (f, g) shows the CD curves of the $NiCo_2O_4$//$NiCo_2O_4$ symmetric supercapacitor cell tested at a current density 6

mA cm^{-1}. The cycling stability results for the symmetric cell indicate that it is suitable for use in symmetric and asymmetric devices (Figure 6f) [69]. The cycling stability values of our symmetric cell are better than those reported for other $NiCo_2O_4$ symmetric cells [69, 70]. Figure 6h shows Nyquist plots of after and before stability for the $NiCo_2O_4$//$NiCo_2O_4$ symmetric supercapacitor, revealing low solution and charge transfer resistance values, thereby indicating that the $NiCo_2O_4$//$NiCo_2O_4$ symmetric supercapacitor exhibits outstanding electrical conductivity [68-72]. The Nyquist plots show a very small semicircle, which specifies that the charge-transfer and solution resistance are very low for the symmetric supercapacitor, which is attributable to the interconnected flower-like flakes in the electrodes enabling good contact between the two $NiCo_2O_4$ electrodes [72]. Figure 6i shows a typical Ragone plot for our $NiCo_2O_4$//$NiCo_2O_4$ symmetric supercapacitors. Our Ragone plot shows the calculated values of an energy density of 7.8 W h kg^{-1} at a power density of 294.54 kW kg^{-1}.

4. Conclusions

In conclusion, innovative $NiCo_2O_4$ thin films were effectively synthesized by the SILAR method at various deposition SILAR cycles. The electrochemical results revealed that the $NiCo_2O_4$ thin films exhibit superior capacitive performance high rate capability, and better cycling stability. The surface morphology and crystal structure investigation confirmed the development of a cubic crystal structure and the formation of different flower-like nanostructures on the flexible substrate of the $NiCo_2O_4$ thin films, which expressively supported their electrochemical performance. The highest specific capacitance values of about 1936 and 680 F g^{-1} were recorded at scan rates of 5 and 100 mV s^{-1}, respectively, along with better stability. Symmetric supercapacitor performance demonstrations the $NiCo_2O_4$ electrode is useful for the practical applications and devices fabrication. This study demonstrated a simple fabrication

method with the variation of deposition cycles, which affected surface morphology as well as electrochemical properties of the $NiCo_2O_4$ thin films.

Acknowledgments

This study was supported by the Dongguk University Research Fund of 2018-2020.

References:

[1] J. Zhang, F. Liu, J. P. Cheng, X. B. Zhang, "Binary nickel−cobalt oxides electrode materials for high performance supercapacitors: influence of its composition and porous nature." *ACS Appl. Mater. Inter.,* 7 (2015): 17630-1764.

[2] A. Sarkar, A. K. Singh, D. Sarkar, G. G. Khan, K. Mandal, "Three dimensional nano-architecture of $BiFeO_3$ anchored TiO_2 nanotube arrays for electrochemical energy storage and solar energy conversion." *ACS Sustain. Chem. Eng.,* 3 (2015): 2254-2263.

[3] A. M. Elshahawy, C. Guan, W. Zang, S. Ding, Z. Kou, S. J. Pennycook, N. Yan, J. Wang, "Phospho-oxynitride layer protected cobalt phosphonitride nanowire arrays for high-rate and stable supercapacitors." *ACS Appl. Ener. Mater.,* 2 (2019): 616-626.

[4] A. Karmakar, S. K. Srivastava, "Interconnected copper cobaltite nanochains as efficient electrocatalysts for water oxidation in alkaline medium." *ACS Appl. Mater. Interf.,* 9 (2017): 22378-22387.

[5] Q. Chu, W. Wang, X. Wang, B. Yang, X. Liu, J. Chen, "Hierarchical $NiCo_2O_4$@nickel-sulfide nanoplate arrays for high performance supercapacitors." *J. Power Source,* 276 (2015): 19-25.

[6] Y. Ji, J. Xie, J. Wu, Y. Yang, X. –Z. Fu, R. Sun, C. –P. Wong, "Hierarchical nanothorns $MnCo_2O_4$ grown on porous/dense Ni bi-layers coated Cu wire current collectors for high performance flexible solid-state fiber supercapacitors." *J. Power Source,* 393 (2018): 54-61.

[7] P. T. Phong, N. X. Phuc, P. H. Nam, N. V. Chien, D. D. Dung, P. H. Linh, "Size-controlled heating ability of $CoFe_2O_4$ nanoparticles for hyperthermia applications." *Phy. B. Cond. Matter.,* 531 (2018): 30-34.

[8] H. Zhang, X. Deng, H. Huang, G. Li, X. Liang, W. Zhou, J. Guo, W. Wei, S. Tang, "Hetero-structure arrays of $NiCoO_2$ nanoflakes@nanowires on 3D graphene/nickel foam for high performance supercapacitors." *Electrochim. Acta,* 289 (2018): 193-203.

[9] C. Zhao, Y. Jin, X. Du, W. Du, "In situ prepared amorphous FeCoO-Polyaniline/multiwalled carbon nanotube nanohybrids as efficient oxygen evolution catalysts for rechargeable Zn-air batteries." *J. Power Source,* 399 (2018): 337-342.

[10] Y. J. Hong, S. –K. Park, K. C. Roh, J. –K. Lee, Y. C. Kang, "Superior electrochemical properties of micron-sized aggregates of $(Co_{0.5}Fe_{0.5})_3O_4$ hollow nanospheres and graphitic carbon." Chem. Eng. J., 346 (2018): 351-360.

[11] S. K. Shinde, M. B. Jalak, G. S. Ghodake, N. C. Maile, V. S. Kumbhar, D. S. Lee, V. J. Fulari, D. -Y. Kim, "Chemically synthesized nanoflakes-like $NiCo_2S_4$ electrodes for high-performance supercapacitor application." Appl. Surf. Sci., 466 (2019): 822-829.

[12] Q. Hou, D. Bacal, A. N. Jumabekov, W. Li, Z. Wang, X. Lin, S. H. Ng, B. Tan, Q. Baod, S. R. Chesman, Y. –B. Cheng, "Back-contact perovskite solar cells with honeycomb-like charge collecting electrodes." *Nano Energy* 50 (2018): 710-716.

[13] H. Zhang, H. Huang, J. Xu, X. Deng, G. Li, X. Liang, W. Zhou, J. Guo, S. Tang, "Hierarchical $NiCoO_2$ single-crystalline nanoflake arrays on Ni foam for supercapacitors and Li-ion batteries application." *J. Alloys Compd.,* 766 (2018): 952-958.

[14] Z. Bai, S. Li, J. Fu, Q. Zhang, F. Chang, L. Yang, J. Luc, Z. Chen, "Metal-organic framework-derived Nickel Cobalt oxysulfide nanocages as trifunctional electrocatalysts for high efficiency power to hydrogen." *Nano Energy* 58 (2019): 680-686.

[15] C. Wei, Y. Huang, M. Chen, J. Yan, W. Yao, X. Chen, "Fabrication of porous nanosheets assembled from $NiCo_2O_4$/NiO electrode for electrochemical energy storage application." *J. Colloid Inter. Sci.,* 504 (2017): 1-11.

[16] R. Shi, J. Wang, Z. Wang, T. Li, Y. –F. Song, "Unique NiFe–$NiCoO_2$ hollow polyhedron as bifunctional electrocatalysts for water splitting." *J. Ener. Chem.,* 33 (2019): 74-80.

[17] X. Yin, G. Sun, L. Su, L. Wang, G. Shao, "Surface roughening of nanoparticle-stacked porous $NiCoO_2$@C microflakes arrays grown on Ni foam for enhanced hydrogen evolution activity." *Electrochim. Acta,* 284 (2018): 226-233.

[18] X. Zhang, S. Yu, W. He, H. Uyama, Q. Xie, L. Zhang, F. Yang, "Electrochemical sensor based on carbon-supported $NiCoO_2$ nanoparticles for selective detection of ascorbic acid." *Biosens Bioelectronics,* 55 (2014): 446-451.

[19] Y. Sun, F. Li, Z. Shen, Y. Li, J. Lang, W. Li, G. Gao, S. Ding, C. Xiao, T. Matsue, "$NiCoO_2$@CMK-3 composite with nanosheets-mesoporous structure as an efficient oxygen reduction catalyst." *Electrochim. Acta,* 294 (2019): 38-45.

[20] X. Tang, B. Zhang, C. Xiao, H. Zhou, X. Wang, D. He, "Carbon nanotube template synthesis of hierarchical $NiCoO_2$ composite for non-enzyme glucose detection." *Sensors Actuators B,* 222 (2016): 232-239.

[21] W. Wang, Y. Yang, Y. Liu, Z. Zhang, W. Dong, Z. Lei, "Hybrid $NiCoO_x$ adjacent to Pd nanoparticles as a synergistic electrocatalyst for ethanol oxidation." *J. Power Sources,* 273 (2015): 631-637.

[22] M. Saraf, K. Natarajan, S. M. Mobin, "Multifunctional porous $NiCo_2O_4$ nanorods: sensitive enzyme less glucose detection and supercapacitor properties with impedance spectroscopic investigations." *New J. Chem.,* 41 (2017): 9299-9313.

[23] Z. Gu, H. Nan, B. Geng, X. Zhang, "Three-dimensional $NiCo_2O_4$@$NiMoO_4$ core/shell nanowires for electrochemical energy storage." *J. Mater. Chem. A.* 3 (2015): 12069-12075.

[24] N. Kumar, P. K. Sahoo, H. S. Panda, "Tuning the electro-chemical properties by selectively substituting transition metals on carbon in Ni/Co oxide–carbon composite electrodes for supercapacitor devices." *New J. Chem.,* 41 (2017): 3562-3573.

[25] B. Saravanakumar, S. S. Jayaseelan, M. –K. Seo, H. –Y. Kim, B. –S. Kim, "$NiCo_2S_4$ nanosheet-decorated 3D, porous Ni film @ Ni wire electrode materials for all solid-state asymmetric supercapacitor applications." *Nanoscale,* 9 (2017): 18819-18834.

[26] H. Tong, S. Yue, L. Lu, F. Jin, Q. Han, X. Zhang, J. Liu, "A binder-free $NiCo_2O_4$ nanosheet/3D elastic N-doped hollow carbon nanotube sponge electrode with high volumetric and gravimetric capacitances for asymmetric supercapacitors." *Nanoscale,* 9 (2017): 16826-16835.

[27] S. Srinivasa Rao, I. K. Durga, N. Kundakarla, D. Punnoose, C. V. V. M. Gopi, A. E. Reddy, M. Jagadeesh, H. –J. Kim, . "A hydrothermal reaction combined with a post anion-exchange reaction of hierarchically nanostructured $NiCo_2S_4$ for high-performance QDSSCs and supercapacitors." *New J. Chem.,* 41 (2017): 10037-10047.

[28] S. Xu, D. Yang, F. Zhang, J. Liu, A. Guo, F. Hou, "Fabrication of $NiCo_2O_4$ and carbon nanotube nano composite films as a high-performance flexible electrode of supercapacitors." *RSC Adv.,* 5 (2015): 74032-74039.

[29] J. Cheng, Y. Lu, K. Qiu, D. Zhang, C. Wang, H. Yan, J. Xu, Y. Zhang, X. Liu, Y. Luo, "Hierarchical multi-villous nickel–cobalt oxide nanocyclobenzene arrays: morphology control and electrochemical supercapacitive behaviors." *Cryst. Eng. Comm.,* 16 (2014): 9735-9742.

[30] J. Liang, K. Xi, G. Tan, S. Chen, T. Zhao, P. R. Coxon, H. –K. Kim, S. Ding, Y. Yang, R. V. Kumar, J. Lu, "Sea urchin-like $NiCoO_2$@C nanocomposites for Li-ion batteries and supercapacitors." *Nano Energy* 27 (2016): 457-465.

[31] X. Li, W. Sun, L. Wang, Y. Qi, T. Guo, X. Zhao, X. Yan, Three-dimensional hierarchical self-supported $NiCo_2O_4$/carbon nanotube core–shell networks as high performance supercapacitor electrodes, *RSC Adv.,* 2015, 5, 7976–7985.

[32] Q. Wang, B. Liu, X. Wang, S. Ran, L. Wang, D. Chen, G. Shen, "Morphology evolution of urchin-like $NiCo_2O_4$ nanostructures and their applications as psuedocapacitors and photoelectro-chemical cells." *J. Mater. Chem.*, 22 (2012): 21647-21653.

[33] S. K. Shinde, G. S. Ghodake, V. J. Fulari, D. -Y. Kim, High electrochemical performance of nanoflakes like CuO electrode by successive ionic layer adsorption and reaction (SILAR) method, J. Ind. Eng. Chem. 52 (2017): 12–17

[34] S. K Shinde, D. P Dubal, G. S Ghodake, D. –Y. Kim, V. J. Fulari, Morphological tuning of CuO nanostructures by simple preparative parameters in SILAR method and their consequent effect on supercapacitors, Nano-Structures & Nano-Objects, 6 (2016): 5-13

[35] S. K. Shinde, M. B. Jalak, G. S. Ghodake, N. C. Maile, H. M. Yadav, A. D. Jagadale, A. Shahzad, D. S. Lee, A. A. Kadam, V. J. Fulari, D. -Y. Kim, Flower-like $NiCo_2O_4$/$NiCo_2S_4$

electrodes on Ni mesh for higher supercapacitor applications, Ceram. Int. 45 (2019): 17192-17203

[36] S. Cho, S. Lee, B. Hou, J. Kim, Y. Jo, H. Woo, S. M. Pawar, A. I. Inamdar, Y. Park, S. N. Cha, H. Kim, H. Im, Optimizing nanosheet nickel cobalt oxide as an anode material for bifunctional electrochemical energy storage and oxygen electrocatalysis, *Electrochim. Acta,* 274 (2018): 279-287.

[37] Ying-Yu Huang, and Lu-Yin Lin. "Synthesis of Ternary Metal Oxides for Battery-Supercapacitor Hybrid Devices: Influences of Metal Species on Redox Reaction and Electrical Conductivity." *ACS Appl. Mater. Interf.,* 1 (2018): 2979-2990.

[38] H. Lai, L. Shang, Q. Wu, L. Yang, J. Zhao, H. Li, Z. Lyu, X. Wang, Z. Hu, . "Spinel nickel cobaltite mesostructures assembled from ultrathin nanosheets for high-performance electrochemical energy storage." *ACS Appl. Energy Mat.,* 1 (2018): 684-691.

[39] R. J. Deokate, R. S. Kalubarme, C. –J. Park, C. D. Lokhande, "Simple Synthesis of $NiCo_2O_4$ thin films using spray pyrolysis for electrochemical supercapacitor application: A Novel approach." *Electrochim. Acta,* 224 (2017): 378-385.

[40] S. Verma, H. M. Joshi, T. Jagadale, A. Chawla, R. Chandra, S. Ogale, "Nearly monodispersed multifunctional $NiCo_2O_4$ spinel nanoparticles: magnetism, infrared transparency, and radiofrequency absorption." *J. Phy. Chem., C,* 112 (2008): 15106-15112.

[41] Y. Mo, Q. Ru, X. Song, L. Guo, J. Chen, X. Hou, S. Hu, "The sucrose-assisted $NiCo_2O_4$@C composites with enhanced lithium storage properties." *Carbon* 109 (2016): 616-623.

[42] H. Zhang, H. Qiao, H. Wang, N. Zhou, J. Chen, Y. Tang, J. Li, C. Huang, "Nickel cobalt oxide/carbon nanotubes hybrid as a high-performance electrocatalyst for metal/air battery." *Nanoscale* 6 (2014): 10235-10242.

[43] D. -Y. Kim, G. S. Ghodake, N. C. Maile, A. A. Kadam, Dae Sung Lee, V. J. Fulari, S. K. Shinde, Chemical Synthesis of Hierarchical $NiCo_2S_4$ Nanosheets Like Nanostructure on Flexible Foil for a High Performance Supercapacitor, *Sci. Rep.,* 7 (2017) 9764–9764.

[44] S. K. Shinde, Sivalingam Ramesh, C. Bathula, G. S. Ghodake, D.-Y. Kim, A. D. Jagadale, A. A. Kadam, D. P. Waghmode, T. V. M. Sreekanth, Heung Soo Kim, P. C. Nagajyothi, H. M. Yadav, Novel approach to synthesize NiCo2S4 composite for high-performance supercapacitor application with different molar ratio of Ni and Co, Scientific Reports, 9 (2019) 13717- 13726.

[45] S. K. Shinde, D. P. Dubal, G. S. Ghodake, V. J. Fulari, "Hierarchical 3D-flower-like CuO nanostructure on copper foil for supercapacitors." *RSC Adv.*, 5 (2015): 4443-4447.

[46] S. K. Shinde, G. S. Ghodake, D. P. Dubal, H. D. Dhaygude, D. –Y. Kim, V. J. Fulari, "Enhanced photoelectrochemical properties of nanoflower-like hexagonal $CdSe_{0.6}Te_{0.4}$: Effect of electron beam irradiation." *J. Ind. Eng. Chem.*, 45 (2017): 92-98.

[47] S. K. Shinde, V. J. Fulari, D. -Y. Kim, N. C. Maile, R. R. Koli, H. D. Dhaygude, G. S. Ghodake, "Chemical synthesis of flower-like hybrid $Cu(OH)_2$/CuO electrode: Application of polyvinyl alcohol and triton X-100 to enhance supercapacitor performance." *Colloid Surf. B. Bio.,* 156 (2017): 165-174.

[48] S. K. Shinde, D. P. Dubal, G. S. Ghodake, D. –Y. Kim, V. J. Fulari, "Nanoflower-like CuO/$Cu(OH)_2$ hybrid thin films: Synthesis and electrochemical supercapacitive properties." *J. Electroanal. Chem.,* 732 (2014): 80-85.

[49] M. Kundu, G. Karunakaran, E. Kolesnikov, V. E. Sergeevna, S. Kumari, M. V. Gorshenkov, D. Kuznetsov, "Hollow $NiCo_2O_4$ nano-spheres obtained by ultrasonic spray pyrolysis method with superior electrochemical performance for lithium-ion batteries and supercapacitors." *J. Ind. Eng. Chem.,* 59 (2018): 90-98.

[50] S. K Shinde, D. P Dubal, G. S. Ghodake, P. G. -Romero, S. Kim, V. J. Fulari, Influence of Mn Incorporation on the Supercapacitive Properties of Hybrid CuO/Cu(OH)2 Electrodes, RSC Adv., 5 (2015) 30478–30484.

[51] S. K. Shinde, D. P. Dubal, G. S. Ghodake, D. Y. Kim, V. J. Fulari, Nanoflower-Like CuO/Cu(OH)2 Hybrid Thin Films: Synthesis and Electrochemical Supercapacitive Properties, J. Electroanal. Chem., 732 (2014) 80–85

[52] N. Jabeen, Q. Xia, M. Yang, H. Xia, "Unique core−shell nanorod arrays with polyaniline deposited into mesoporous $NiCo_2O_4$ support for high-performance supercapacitor electrodes", *ACS Appl. Mater. Interf.,* 8 (2016): 6093-6100.

[53] Y. Yang, D. Zeng, S. Yang, L. Gu, B. Liu, S. Hao, "Nickel cobaltite nanosheets coated on metal-organic framework-derived mesoporous carbon nanofibers for high-performance pseudocapacitors." *J. Colloid Interf. Sci.,* 534 (2019): 312-321.

[54] Y. Tao, L. Ruiyi, Li Zaijun, F. Yinjun, "A facile and scalable strategy for synthesis of size-tunable $NiCo_2O_4$ with nanocoral-like architecture for high-performance supercapacitors." *Electrochim. Acta,* 134 (2014): 384-392.

[55] Y. Zhang, Z. Guo, "Honeycomb-like $NiCo_2O_4$ films assembled from interconnected porous nanoflakes for supercapacitor." *Mater. Chem. Phys*, 171 (2016): 208-215.

[56] J. Du, G. Zhou, H.M. Zhang, C. Cheng, J.M. Ma, W.F. Wei, L.B. Chen, T.H. Wang, "Ultrathin porous $NiCo_2O4$ nanosheet arrays on flexible carbon fabric for high-performance supercapacitors." *ACS Appl. Mater. Interf.,* 5 (2013): 7405-7409.

[57] H. Wang, J. Lu, S. Yao, W. Zhang, "Sodium dodecyl sulfate-assisted synthesis of flower-like $NiCo_2O_4$ microspheres with large specific surface area for supercapacitors", *J. Alloy Compd.*, 744 (2018): 187-195.

[58] K. Xu, S. Ma, Y. Shen, Q. Ren, J. Yang, X. Chen, J. Hu, "$CuCo_2O_4$ nanowire arrays wrapped in metal oxide nanosheets as hierarchical multicomponent electrodes for supercapacitors", *Chem. Eng. J.*, 369 (2019) 363–369.

[59] F. Yang, K. Xu, J. Hu, "Hierarchical multicomponent electrode with $NiMoO_4$ nanosheets coated on Co_3O_4 nanowire arrays for enhanced electrochemical properties", *J. Alloy Compd.*, 781 (2019) 1127-1131.

[60] F. Yang, K. Xu, J. Hu, "Construction of Co_3O_4@Fe_2O_3 core-shell nanowire arrays electrode for supercapacitors", *J. Alloy Compd.*, 729 (2017) 1172-1176.

[61] J. Wang, L. Zhang, X. Liu, X. Zhang, Y. Tian, X. Liu, J. Zhao, Y. Li, Assembly of flexible $CoMoO_4$@$NiMoO_4$ H2O and Fe_2O_3 electrodes for solid-state asymmetric supercapacitors, Sci. Rep., 7 (2017) 41088-41099.

[62] S. Sarkar, P. Howli, U. K. Ghorai, B. Das, M. Samanta, N. S. Das, and K. K. Chattopadhyay, Flower-like Cu_2NiSnS_4 microspheres for application as electrodes of asymmetric supercapacitors endowed with high energy density, Cryst. Eng. Comm., 20 (2018) 1443-1454.

[63] S. Kaipannan, S. Marappan, Fabrication of 9.6 V High-performance asymmetric supercapacitors stack based on nickel hexacyanoferrate-derived $Ni(OH)_2$ nanosheets and bio-derived activated carbon, Sci. Rep., 9 (2019) 1104-1118.

[64] S. T. Senthilkumar, Y. Wang, H. Huang, Advances and prospects of fiber supercapacitors, J. Mater. Chem. A, 3 (2015) 20863–20879.

[65] C. Zhang, X. Cai, Y. Qian, H. Jiang, L. Zhou, B. Li, L. Lai, Z. Shen, W. Huang, Electrochemically synthesis of nickel cobalt sulfide for high-performance flexible asymmetric supercapacitors, Adv. Sci., 5 (2018) 1700375-1700387.

[66] N. Ahmed, B. A. Ali, M. Ramadan, N. K. Allam, Three-Dimensional Interconnected Binder-Free Mn−Ni−S nanosheets for high performance asymmetric supercapacitor devices with exceptional cyclic stability, ACS Appl. Energy Mater. 5 (2019) 3717-3725.

[67] X. Li, J. Shen, W. Sun, X. Hong, R. Wang, X. Zhao, X. Yan, A super-high energy density asymmetric supercapacitor based on 3D core–shell structured NiCo-layered double hydroxide@carbon nanotube and activated polyaniline-derived carbon electrodes with commercial level mass loading, J. Mater. Chem. A, 3 (2015) 13244–13253.

[68] C. –S. Dai, P. –Y. Chien, J. –Y. Lin, S. –W. Chou, W. –K. Wu, P. –H. Li, K. –Y. Wu, T. –W. Lin, Hierarchically structured Ni_3S_2/Carbon nanotube composites as high performance cathode materials for asymmetric supercapacitors, ACS Appl. Mater. Interfaces, 5 (2013) 12168−12174.

[69] M. B. Askari, P. Salarizadeh, Superior catalytic performance of $NiCo_2O_4$ nanorods loaded rGO towards methanol electro-oxidation and hydrogen evolution reaction, J. Mol. Liq., 291 (2019) 111306-111314.

[70] N. Zhao, H. Fan, J. Ma, M. Zhang, C. Wang, H. Li, X. Jiang, X. Cao, Entire synergistic contribution of electrodeposited battery-type $NiCo_2O_4$@$Ni_{4.5}Co_{4.5}S_8$ composite for high-performance supercapacitors, J. Power Sources, 439 (2019) 227097-227107.

[71] X. Wang, Y. Fang, B. Shi, F. Huang, F. Rong, R. Que, Three-dimensional $NiCo_2O_4$@$NiCo_2O_4$ core–shell nanocones arrays for high-performance supercapacitors, Chem. Eng. J., 344 (2018) 311-319.

[72] O. Geuli, Q. Hao, D. Mandler, One-step fabrication of NiOx-decorated carbon nanotubes-NiCo2O4 as an advanced electroactive composite for supercapacitors, Electrochim. Acta, 318 (2019) 51-60.

Conflict of Interest:

I declare that I have no significant competing financial support.

Figure captions

Figure 1 (a) XRD pattern, (b) XPS survey spectrum, (c) Ni 2p narrow scan spectrum, (d) Co 2p narrow scan spectrum, and (e) O1s narrow scan spectrum of optimized $NiCo_2O_4$ thin film.

Figure 2 (a-f) FE-SEM images of the $NiCo_2O_4$ thin films, and (g-i) EDS images of the $NiCo_2O_4$ thin films prepared at various deposition cycles, respectively.

Figure 3 (a-c) TEM images of the $NiCo_2O_4$ thin films prepared at various deposition cycles, (d-f) HE-TEM images of optimized $NiCo_2O_4$ thin films with different magnifications, (g) Seed pattern, and (h-k) Elemental mapping of the optimized $NiCo_2O_4$ thin films, respectively.

Figure 4 (a–c) CV curves of the $NiCo_2O_4$ thin film prepared at various deposition cycles with different scan rates from 5 to 100 mVs^{-1} in the potential window from –0.1 to 0.5 V, and (d) specific capacitance of the $NiCo_2O_4$ thin film prepared using the chemical method.

Figure 5 (a–c) GCD curves and (d) Specific capacitance of the $NiCo_2O_4$ thin film prepared at various deposition cycles with different current densities from 10 to 35 mA cm^{-1} in 3 M KOH, respectively, (e) Cycling stability of the optimized $NiCo_2O_4$ thin film, (f) EIS tests of the $NiCo_2O_4$ thin films prepared at various deposition cycles.

Figure 6 (a) Schematic design of symmetric (SS) supercapacitor devices fabrication, (b, c) CV curves and specific capacitance of devices with various scan rates, respectively (d, e) GCD curves and specific capacitance at different current density from 6-10 mA cm^{-2}, respectively, (f) Stability of symmetric (SS) supercapacitor upto first 10 cycle with potential range 0 to 0.6 V, (g) GCD curves of first and 500 cycle, (h) Nyquist plots of the before and after testing stability, (i) Ragone plot of symmetric (SS) supercapacitor devices.

Table 1 EIS parameters of NCo_2O_4 thin films prepared at different deposition cycles by SILAR method

Sample D/Parameters	*NCO:A*	*NCO:B*	*NCO:C*
R_s (Ω)	2.9	1.94	3.8
C	00007906	1.257	2,131E-5
R_{ct} (Ω)	8.6	3.2	4.6
W	0,2892	4,317E4	0,1194
∑R (Ω)	*11.5*	*5.14*	*8.4*

Graphical Abstract:

Figure (a) TEM of chain like nanoflowers, (b) Cycling stability, insert shows the FE-SEM of before and after testing electrochemical testing of $NiCo_2O_4$ thin films.

❖ Highlights

- Simple and room temperature chemical synthesis method are employed for modification in surface morphology.
- The $NiCo_2O_4$ film showed highest specific capacitance of 1936 F g^{-1} at a scan rate of 5 mV s^{-1}.
- The $NiCo_2O_4$ showed excellent supercapacitor applications.
- The synergistic effect between deposition cycles on electrochemical performance and surface morphologies of $NiCo_2O_4$ thin fillms.

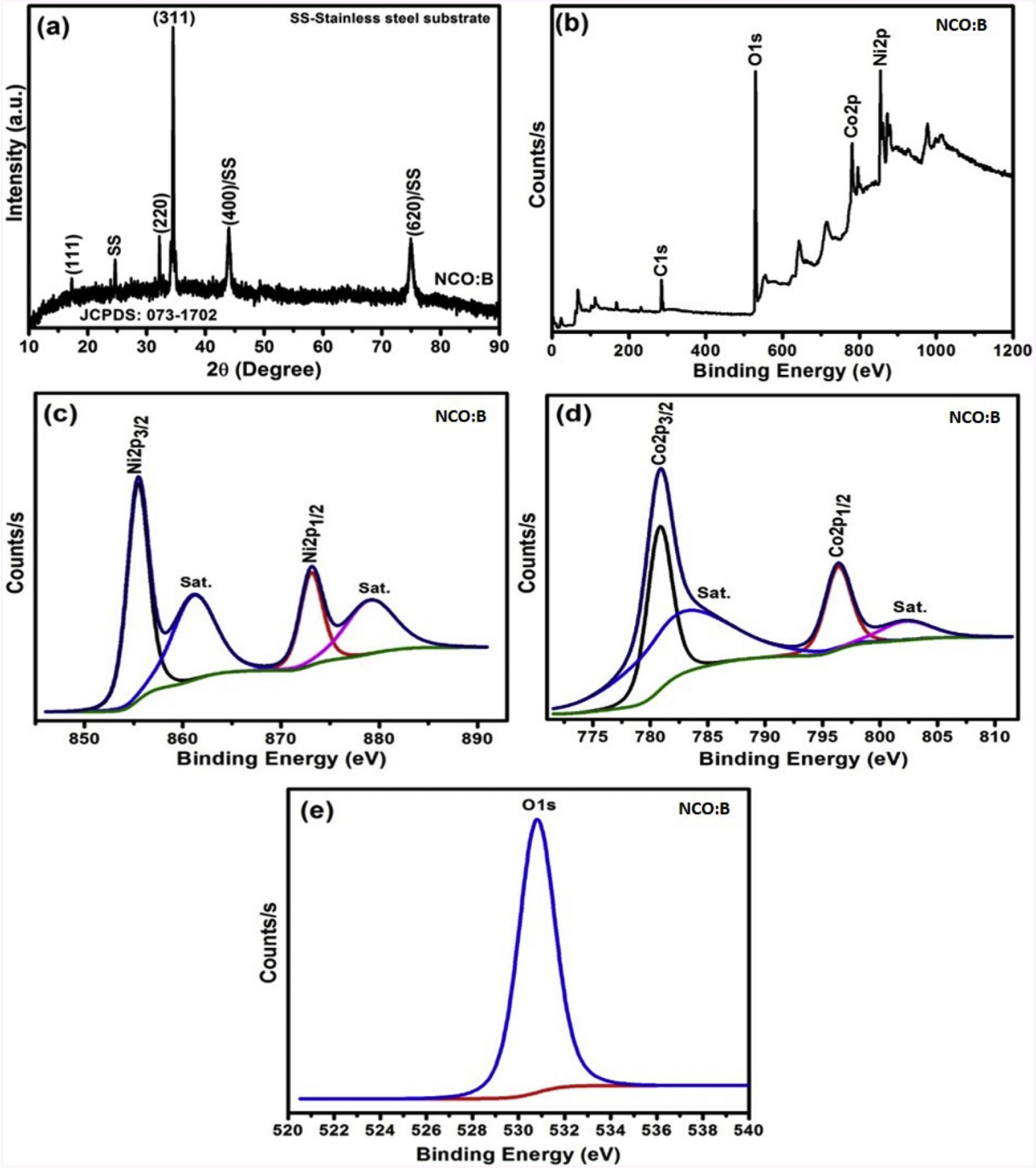
(a)
SS-Stainless steel substrate
(311)
(111)
SS
(220)
(400)/SS
(620)/SS
NCO:B
JCPDS: 073-1702
Intensity (a.u.)
2θ (Degree)
(b)
NCO:B
O1s
Ni2p
Co2p
C1s
Counts/s
Binding Energy (eV)
(c)
NCO:B
Ni2p3/2
Ni2p1/2
Sat.
Sat.
Counts/s
Binding Energy (eV)
(d)
NCO:B
Co2p3/2
Co2p1/2
Sat.
Sat.
Counts/s
Binding Energy (eV)
(e)
O1s
NCO:B
Counts/s
Binding Energy (eV)

Figure 1

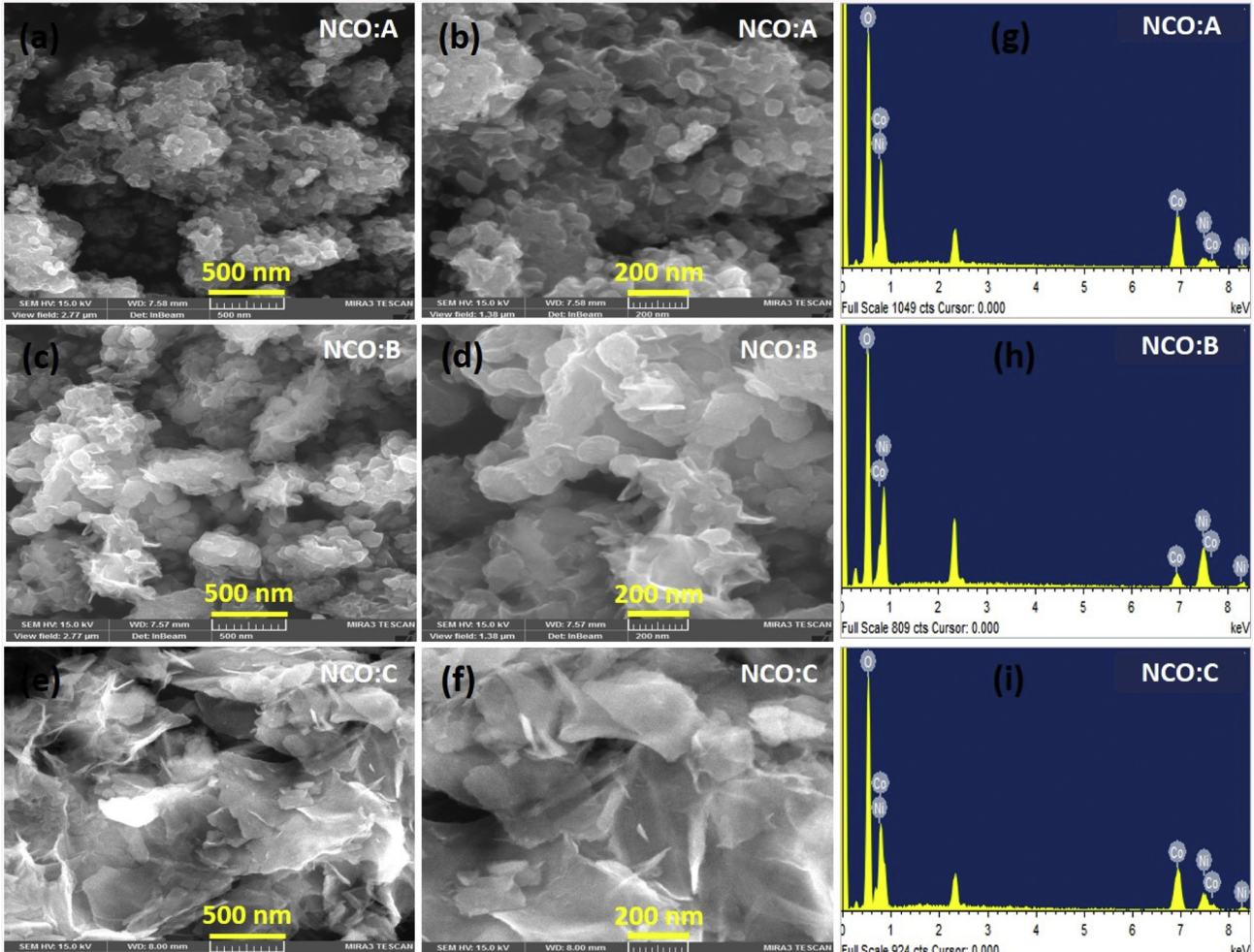
(a)
NCO:A
500 nm
(b)
NCO:A
200 nm
(g)
NCO:A
O
Co
Ni
Full Scale 1049 cts Cursor: 0.000
keV
(c)
NCO:B
500 nm
(d)
NCO:B
200 nm
(h)
NCO:B
Full Scale 809 cts Cursor: 0.000
keV
(e)
NCO:C
500 nm
(f)
NCO:C
200 nm
(i)
NCO:C
Full Scale 924 cts Cursor: 0.000
keV

Figure 2

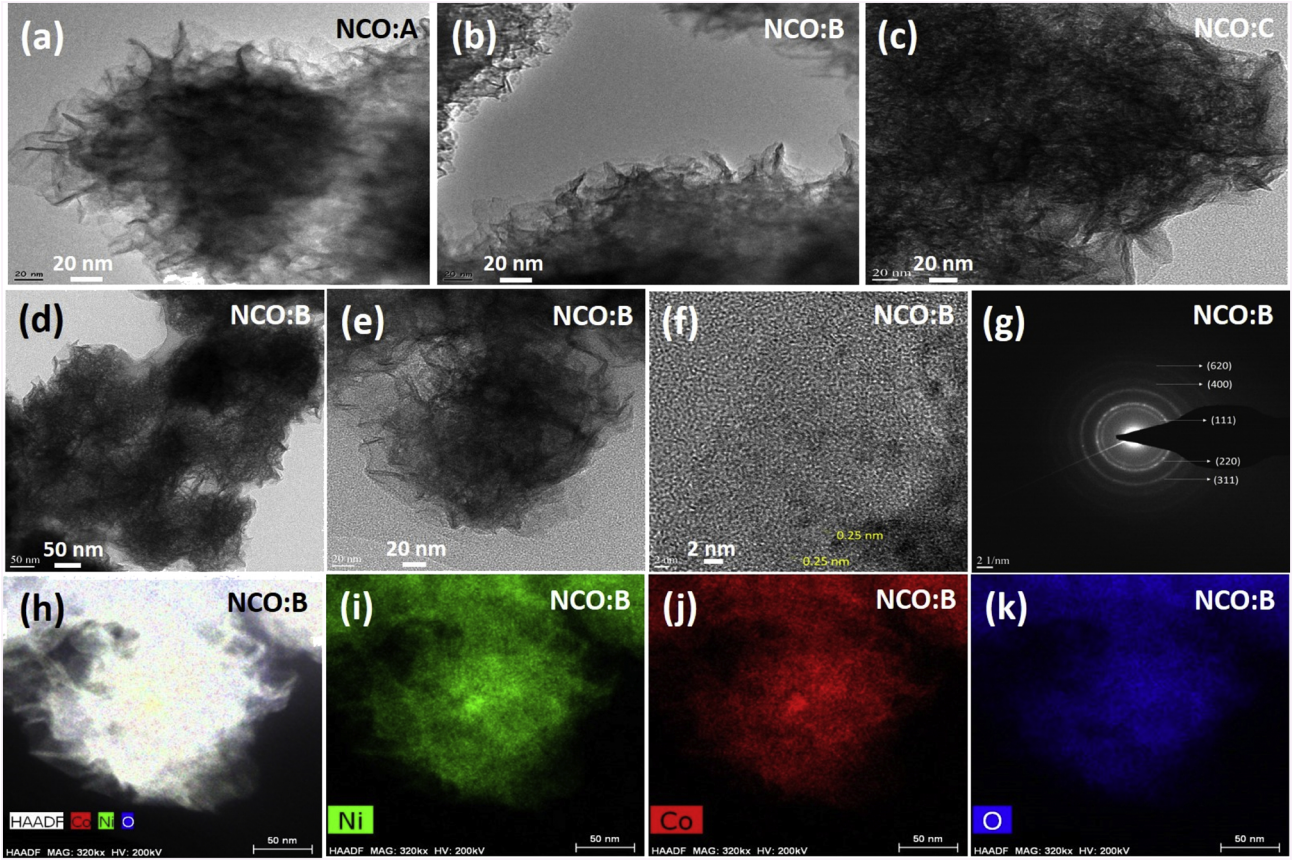
(a)
NCO:A
20 nm
(b)
NCO:B
20 nm
(c)
NCO:C
20 nm
(d)
NCO:B
50 nm
(e)
NCO:B
20 nm
(f)
NCO:B
2 nm
0.25 nm
0.25 nm
(g)
NCO:B
(620)
(400)
(111)
(220)
(311)
2 1/nm
(h)
NCO:B
HAADF Co Ni O
HAADF MAG: 320kx HV: 200kV
50 nm
(i)
NCO:B
Ni
HAADF MAG: 320kx HV: 200kV
50 nm
(j)
NCO:B
Co
HAADF MAG: 320kx HV: 200kV
50 nm
(k)
NCO:B
O
HAADF MAG: 320kx HV: 200kV
50 nm

Figure 3

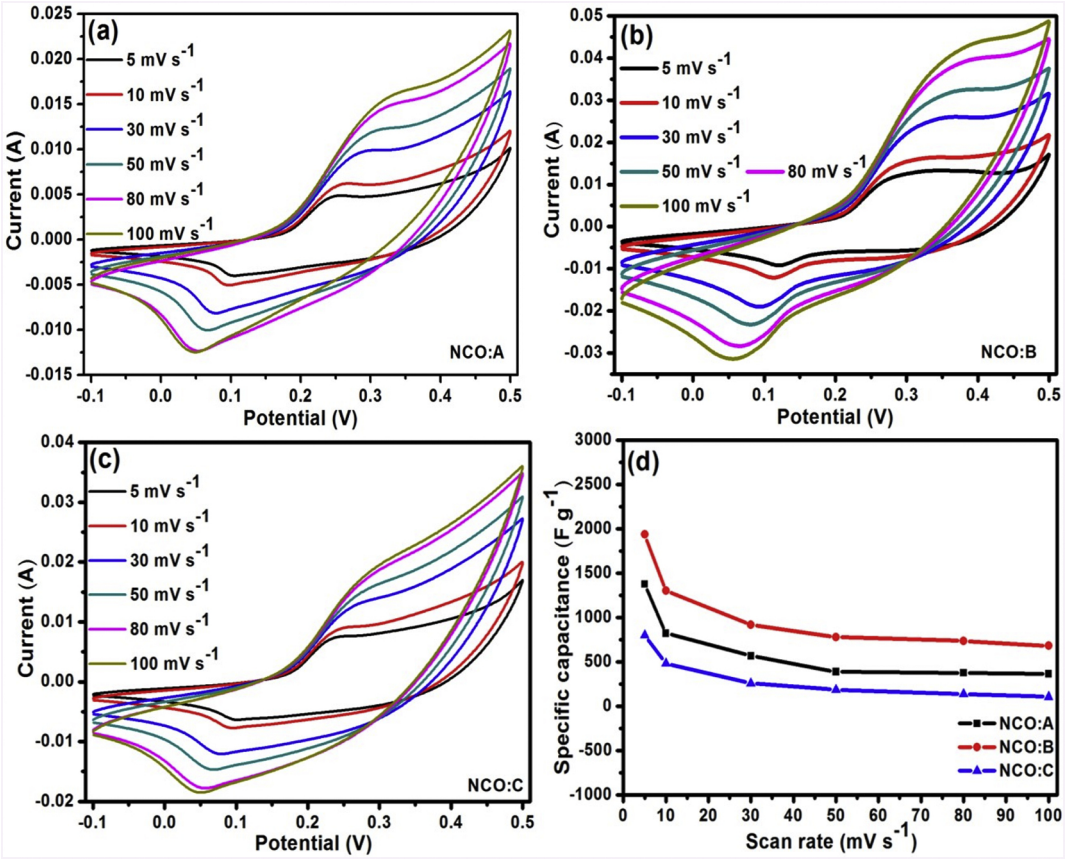
(a)
5 mV s-1
10 mV s-1
30 mV s-1
50 mV s-1
80 mV s-1
100 mV s-1
NCO:A
Current (A)
Potential (V)
(b)
NCO:B
(c)
NCO:C
(d)
Specific capacitance (F g-1)
Scan rate (mV s-1)
NCO:A
NCO:B
NCO:C

Figure 4

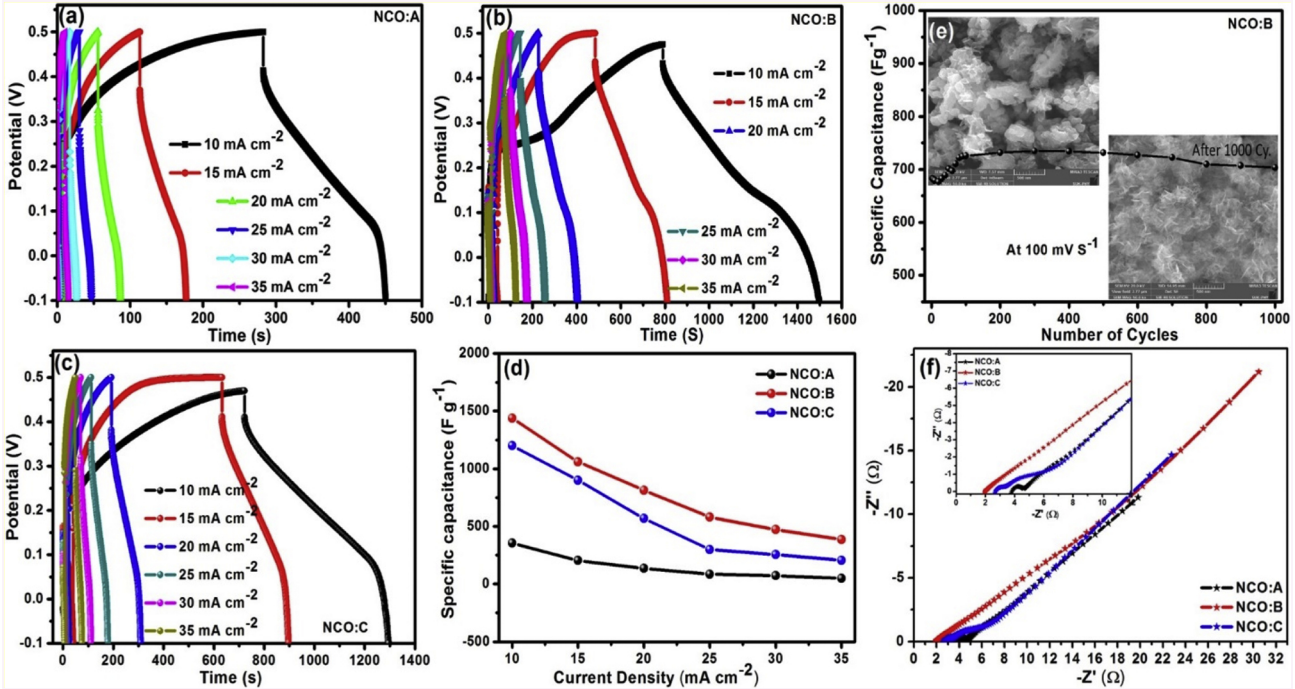
(a)
NCO:A
Potential (V)
Time (s)
10 mA cm-2
15 mA cm-2
20 mA cm-2
25 mA cm-2
30 mA cm-2
35 mA cm-2
(b)
NCO:B
Potential (V)
Time (S)
10 mA cm-2
15 mA cm-2
20 mA cm-2
25 mA cm-2
30 mA cm-2
35 mA cm-2
(e)
NCO:B
Specific Capacitance (Fg-1)
Number of Cycles
At 100 mV S-1
After 1000 Cy.
(c)
Potential (V)
Time (s)
10 mA cm-2
15 mA cm-2
20 mA cm-2
25 mA cm-2
30 mA cm-2
35 mA cm-2
NCO:C
(d)
Specific capacitance (F g-1)
Current Density (mA cm-2)
NCO:A
NCO:B
NCO:C
(f)
-Z'' (Ω)
-Z' (Ω)
NCO:A
NCO:B
NCO:C

Figure 5

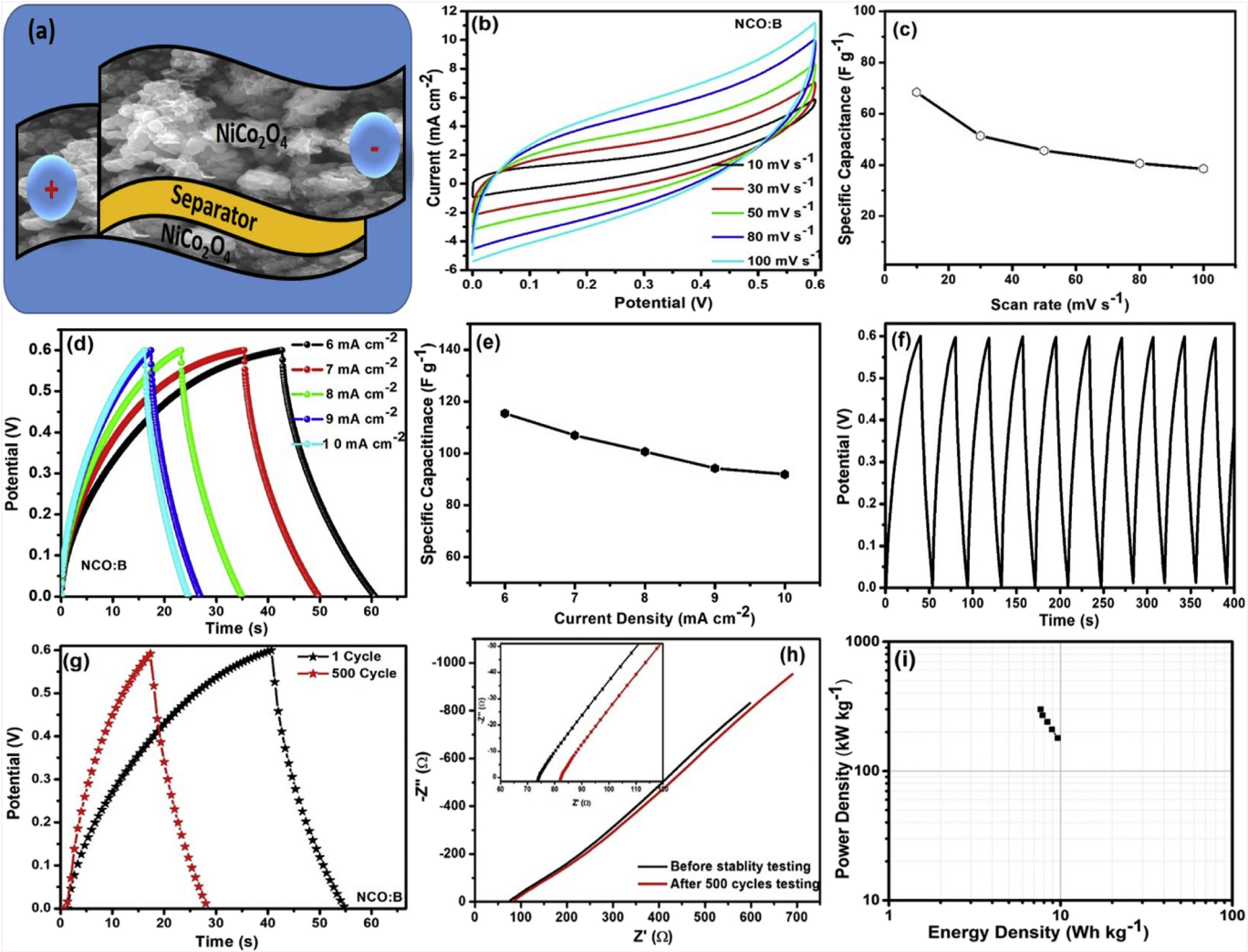
(a)
NiCo2O4
Separator
NiCo2O4
+
-
(b)
NCO:B
Current (mA cm-2)
Potential (V)
10 mV s-1
30 mV s-1
50 mV s-1
80 mV s-1
100 mV s-1
(c)
Specific Capacitance (F g-1)
Scan rate (mV s-1)
(d)
6 mA cm-2
7 mA cm-2
8 mA cm-2
9 mA cm-2
1 0 mA cm-2
Potential (V)
Time (s)
NCO:B
(e)
Specific Capacitinace (F g-1)
Current Density (mA cm-2)
(f)
Potential (V)
Time (s)
(g)
1 Cycle
500 Cycle
Potential (V)
Time (s)
NCO:B
(h)
-Z'' (Ω)
Z' (Ω)
Before stablity testing
After 500 cycles testing
(i)
Power Density (kW kg-1)
Energy Density (Wh kg-1)

Figure 6